



Copper tantalum nitride (CuTaN₂) thin films prepared by reactive radio-frequency magnetron sputtering

Md Maidul Islam¹ · Abhishek Goud Ranga² · Vamsi Borra² · Daniel G. Georgiev¹

Received: 9 January 2024 / Accepted: 23 April 2024
© The Author(s) 2024

Abstract

RF reactive sputtering was used to deposit copper tantalum nitride (CuTaN₂) films from a Cu/Ta target in an environment containing a mixture of argon and nitrogen at two different substrate temperatures: room temperature and 200 °C. The films were studied by SEM, EDS, XRD, Raman spectroscopy, spectrophotometry, and resistivity measurements. The deposition conditions significantly impacted the morphology of the films, which varied from smooth, void-free films at high nitrogen concentrations and at room temperature substrates to cauliflower-like grains with voids at low nitrogen contents and elevated substrate temperatures. Despite the target's 1:1 Cu: Ta ratio, the stoichiometric analysis showed a lower Ta content in the deposited film. The films produced on silicon substrates were polycrystalline, whereas those deposited on glass substrates were amorphous. The band gap (0.9 eV to 1.55 eV) and film resistivity (20 kΩ-cm to 76 kΩ-cm) are strongly affected by the nitrogen fraction in the sputtering gas. Increasing the nitrogen percentage in semiconductor films results in smoother films with larger bandgaps (approximately 1.5 eV), higher resistivity, and compositions closest to those of stoichiometric CuTaN₂.

Keywords Copper tantalum nitride · Thin films · RF reactive sputtering · Scanning electron microscopy · X-ray diffraction · Raman spectroscopy · Band gap · Resistivity measurements

1 Introduction

Nitride semiconducting compounds have attracted substantial interest due to their competitive semiconductor properties and the availability of environmentally friendly precursors and processing methods [1]. Despite their promising attributes, nitrides have been studied less than their oxide counterparts, constituting only approximately 30% of the published combined oxide and nitride research [2]. Thus, there is room for further investigation and development in the realm of nitride semiconductors. Semiconducting nitrides, with their intermediate electronegativity of the N atom (3.0), are of general interest for optoelectronic

applications due to their unique combination of covalent and ionic bonding characteristics [3]. The proximity of the constituent atomic orbitals to the band margins enables greater tolerance for structural defects than does the proximity of other group 15 elements (old group VII). Additionally, their ionic nature allows for effective scaling up of in-line sputtered nitride films, making them suitable for low-cost fabrication. Examples include transition metal nitrides such as titanium nitride in wear-resistant coatings and architectural glass [2].

This group of semiconductors encompasses a wide range of binary and multielement compounds, and some of these compounds have been extensively researched for their unique properties. Among them, gallium nitride (GaN), aluminum nitride (AlN), and indium nitride (InN) are well-established and widely used in various applications [4]. On the other hand, other binary nitride compounds, such as copper nitride (Cu₃N), exhibit significant compositional and structural variations, are less well understood, and are subject to current interest [5–10]. The related ternary nitrides are categorized as having an anti-perovskite structure (Cu₃M_xN), a delafossite structure, a bent -Cu-N- nitridocuprate structure,

✉ Md Maidul Islam
MdMaidul.Islam@rockets.utoledo.edu

¹ Department of Electrical Engineering and Computer Science, The University of Toledo, Toledo, OH 43606, USA

² Electrical and Computer Engineering Program, Rayen School of Engineering, Youngstown State University, Youngstown, OH 44555, USA

or a mixed complex nitridocuprate anion structure [1]. Among these materials, anti-perovskite and delafossite have attracted the most attention for semiconductor applications.

In the anti-perovskite structure, characterized by a customary cubic anti- ReO_3 arrangement, the Cu_3N crystal contains copper atoms positioned at the centers of the edges. These copper atoms establish linear connections with the two closest nitrogen (N) atoms. Since the structure of Cu_3N is similar to that of an anti-perovskite, the ability of copper to create anti-perovskite nitrides is expected. Occupying the cubic body center turns anti- ReO_3 copper(I) nitride into a perovskite. This family is usually expressed as Cu_3NM_x , where M can consist of different proportions ($0 < x < 1$) of alkali metals, such as lithium; transition metals, such as Ti, Pb, Ni, Zn, Cr, Fe, Mn, Al, and Sc; or nonmetals, such as H and O [11]. This kind of structure is sometimes described as doped Cu-N in the literature [1]. On the other hand, the delafossite structure comprises layers of metal cations separated by layers of anions (details in Sect. 0). The delafossite structure is well known in the field of p-type transparent conducting oxides (TCOs) because the archetype material CuAlO_2 is a delafossite [12].

Szymanski et al. investigated nitride delafossite, which included CuTaN_2 , CuNbN_2 , AgTaN_2 , AgNbN_2 , AgVN_2 , AuTaN_2 , and AuNbN_2 [13]. Among these, copper tantalum nitride (CuTaN_2) has been identified as the most promising environmentally benign and earth-abundant semiconductor. Henceforth, CTN is used as the abbreviation for CuTaN_2 . The initial report on delafossite CTN was in 1991, in which only fundamental structural properties were provided [14]. In recent years, researchers have increasingly focused on comprehensively exploring the properties of these materials, particularly from the perspective of their potential as semiconductors, including for use in solar cells. This exploration has predominantly involved computational approaches [2, 13], with relatively few experimental investigations [15]. Furthermore, compared to other well-known delafossite nitrides, CTN exhibits promising attributes, indicating its high potential for application in solar cells and optoelectronic devices [13].

Regarding preparation methods, ion exchange has been used to create the archetypal nitride delafossite CTN in bulk form since 1991 [14, 15]. Overall, both experimental and theoretical studies suggested that the material possessed an indirect band gap of close to 1.3 eV and, therefore, a significant optical absorption in the range of 1.4–1.5 eV [13]. The calculations also indicate that the absorption coefficient of CTN is more than 10^5 cm^{-1} above 1.5 eV, which is desirable in solar cell applications since thinner films are needed to absorb most of the sunlight [2].

CTN has significant advantages over traditional group-IV, III–V, and II–IV semiconductors, including earth abundance,

chemical stability under operating circumstances, and large-scale low-temperature fabrication methods [15]. However, the literature lacks reports concerning the sputter deposition of CTN thin films. The sputtering thin-film deposition method is known for its ability to precisely control film characteristics, efficient material use, versatility for various materials, and suitability for heat-sensitive materials. It is widely used in microelectronics and optics, offering cost-effective, quality thin film production [16, 17]. In this work, thin films were obtained through reactive sputtering using a Cu-Ta alloy target in a controlled nitrogen and argon atmosphere. A systematic variation of the nitrogen fraction in the argon and nitrogen gas mixture within the sputtering chamber was used while the substrate was at room temperature for one set of samples and at 200 °C for another. The effects of varying these deposition parameters are examined by SEM, XRD, EDX, Raman spectroscopy, spectrophotometry, and four-point probe resistivity measurements.

2 Experimental

Copper tantalum nitride thin films were deposited on glass and Si (100) substrates using RF magnetron sputtering. Factory-cleaned substrates were subjected to further cleaning using a process involving distilled water and Micro90 cleaning solution, along with ultrasonic treatment in acetone and alcohol. The deposition was performed in a Torr International system using a 2-inch disc target of 99.9% pure copper and tantalum alloy consisting of 50% Cu and 50% Ta (from Plasmaterials) [18]. The substrates were positioned on a rotating substrate holder approximately 15 cm above the target surface. Before the sputtering process, the vacuum chamber was pumped down to a pressure less than 10^{-7} Torr using an oil-free mechanical pump and a turbomolecular pump. The chamber was purged with ultrahigh purity argon to minimize oxygen and moisture content. A range of thin-film samples was fabricated using nitrogen gas fractions (the ratio of nitrogen gas flow to the total argon and nitrogen gas flow) of 0.2, 0.4, 0.5, 0.6, and 0.8, designated 0.2 N, 0.4 N, 0.5 N, 0.6 N, and 0.8 N, respectively. Two sets of samples were prepared. The substrates of the first set of samples remained unheated (referred to as room-temperature samples).

In contrast, the substrates of the second set of samples were heated to 200 °C during deposition. In both cases, the sputtering procedure was conducted using an RF power level of 100 W. Before each deposition, the target underwent a pre-sputtering phase for a minimum of 10 min with the same power in ultrahigh purity argon. The sputtering gas mixture included high-purity nitrogen and argon (99.9997% purity from Airgas). The deposition chamber pressure was

maintained at 12 mTorr. Real-time film thickness monitoring was performed using a quartz monitor, and the final film thickness was confirmed to be approximately 300 nm by postdeposition SEM cross-sectional imaging.

The films were studied by scanning electron microscopy (SEM), conducted with a Hitachi S-4800 high-resolution scanning electron microscope, and equipped with an energy-dispersive X-ray spectrometer (EDX) to assess chemical composition. Four-point probe electrical measurements were taken with a Signatone Pro4 resistivity test system to determine the material's resistivity. Optical spectrophotometry was performed by using a Lambda 1050 Spectrophotometer. The optical band gap was then calculated from the obtained spectra. The crystallinity of the films was assessed by parallel-beam X-ray diffraction (XRD) utilizing a Rigaku Ultima III X-ray diffractometer system equipped with a Cu K α radiation inline focus, an X-ray mirror, and a 0.5° parallel plate collimator. Raman spectroscopy (RS) was performed utilizing an iHR320 (Horiba Scientific) mid-focal length spectrometer equipped with a microscope. The measurements employed a green light laser emitting at a wavelength of 531.4 nm, with power levels of 50 mW and exposure time of 500s.

3 Results and discussion

This section discusses the characterization results and observed trends as a function of the nitrogen fraction in the sputtering gas mixture for the two substrate temperature cases.

3.1 Film morphology and deposition rate

As shown in (Fig. 1), the films deposited at room temperature displayed a consistent, semispherical, and uniform cauliflower-like structure, which strongly resembled those previously observed in tantalum nitride films [19]. The

grains manifest a comparatively larger size at a low N fraction, yielding heightened film surface roughness. Remarkably, examination of the larger grains revealed evidence of conglomeration of smaller grains, as evidenced by readily observable smaller grain boundaries within their structure. A lower nitrogen content in the sputtering gas mixture leads to greater grain growth, resulting in irregular surface morphology and the observed conglomeration at the grain level [20]. In contrast, as the nitrogen fraction increases, a significant reduction in both grain size and film surface roughness is observed, ultimately yielding a more featureless, smoother film surface. Introducing a higher nitrogen fraction likely facilitates changes in the crystalline structure and growth dynamics during deposition. Nitrogen may influence the nucleation and growth of grains, resulting in smaller and more compact structures on the film surface.

On the other hand, thin films deposited at 200 °C exhibited significantly larger and better-defined spherical grains. Notably, increased void spaces were observed in films prepared at 0.2 N, 0.5 N, and 0.6 N, which became more prevalent with increasing nitrogen fraction. Interestingly, the films deposited at 0.8 N had smaller, nonspherical grains characterized by the least void space and a compact, irregular morphology similar to what is observed at room temperature.

The relationship between the deposition rates and N fraction of the films are provided in (Fig. 2) The thicknesses were estimated for these measurements by calculating the average value from multiple locations within the images. The thicknesses were then divided by the deposition time to calculate the deposition rate. The deposition rate was greater for higher substrate temperatures. A consistent trend emerges from this dataset for both deposition temperature cases, revealing an almost linear decrease in the deposition rate with increasing N fraction when the other deposition parameters are fixed. The introduction of nitrogen into the sputtering process leads to chemical reactions with target materials such as tantalum and copper, forming nitride

Fig. 1 Top-view SEM images of films on Si substrates

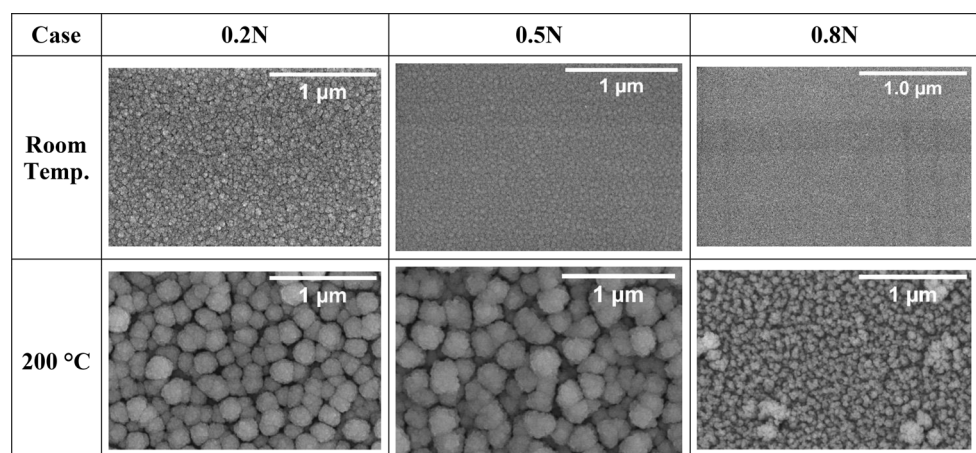


Fig. 2 Dependence of the deposition rate on the N fraction in the sputtering gas mixture (a) Room temperature case (b) 200 °C case

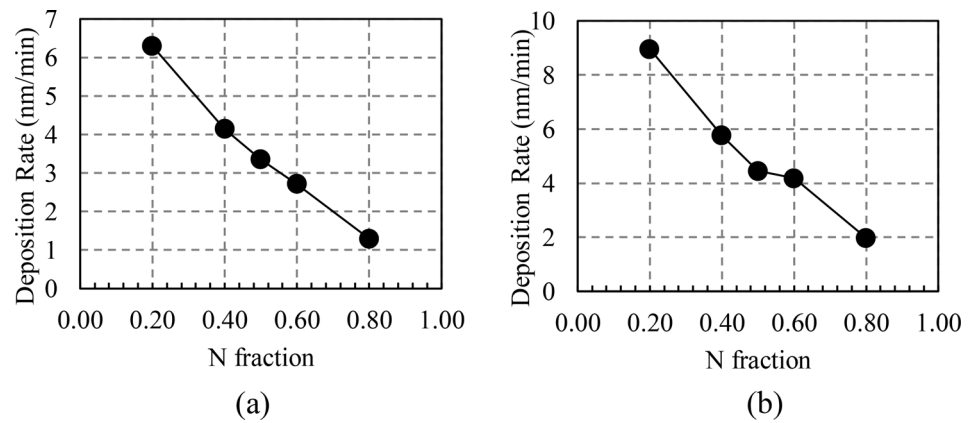
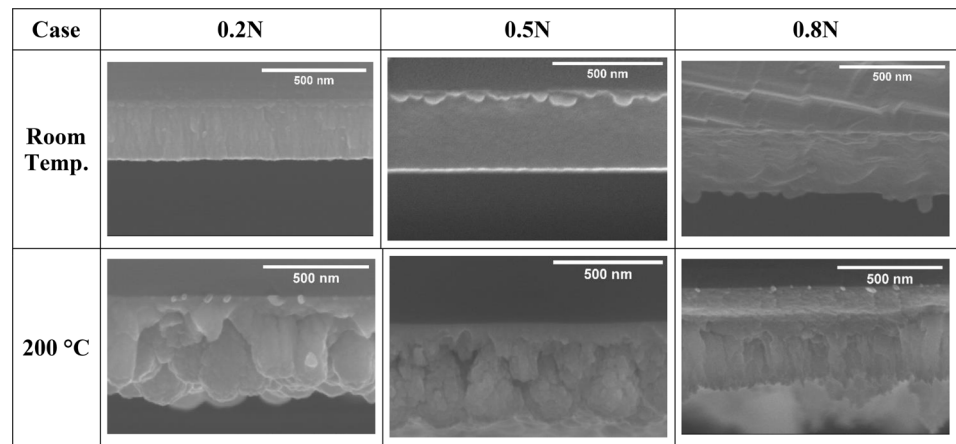


Fig. 3 Cross-sectional view SEM images of films on Si substrates. The substrate is on top



compounds [5, 19]. These reactions often reduce the deposition rate compared to pure metal components, resulting in a diminished sputter yield and overall deposition rate. In addition, the variation in the deposition rate can be related to the fact that argon atoms are heavier than nitrogen atoms, leading to higher sputtering yields in an argon-rich atmosphere.

The cross-sectional imaging revealed pronounced columnar growth within the thin film. The columnar structure is more prevalent for low N fractions, and as the N fraction increases, this distinct columnar morphology becomes less pronounced. The least columnar growth was found for the room temperature and 0.8 N fraction samples. The shift in growth patterns can be attributed to variations in deposition rate [20]. At lower N fractions with a higher deposition rate, atoms have limited time for nucleation during deposition, favoring columnar growth due to constrained mobility. Conversely, even with the same atom mobility at lower deposition rates, atoms gain more time to diffuse, promoting a noncolumnar growth pattern. Additionally, for the 200 °C deposition temperature, the surface SEM images of the samples prepared with gas fractions of 0.2 N, 0.5 N, and 0.6 N demonstrated the presence of voids, which were also detectable in the corresponding cross-sectional images. (Fig. 3)

3.2 Chemical composition

As mentioned above, a target containing 50% Cu and 50% Ta was used to attain a Cu/Ta ratio as close to 1:1 in the film material [18]. The inherent ternary nature of CTN continues to pose challenges for achieving stoichiometric properties through sputtering deposition. The elemental composition of the sputtered CTN thin films on Si substrates was determined using energy dispersive X-ray spectroscopy (EDX), and the results are provided in Table 1. These EDX measurements were conducted at various locations on the sample surface deposited on the Si substrates, and these data were subsequently averaged to obtain representative atomic composition information. At room temperature, the standard deviations (SDs) of elemental compositions are determined to be 0.18, 0.16, and 1.01 atomic % for copper (Cu), tantalum (Ta), and nitrogen (N), respectively. Similarly, at a deposition temperature of 200 °C, these values increase to 0.40, 0.59, and 1.56 atomic % for Cu, Ta, and N, respectively. The SDs calculated are specific to elemental compositions, not numerical ratios. For instance, in the room temperature (RT) and 0.2 N fraction scenario, the SD for copper was 0.10%, with an elemental composition of 6.41%. In this case, tantalum (Ta) exhibited a composition of 4.96%, resulting in a

Table 1 Chemical composition of the films deposited based on EDX data

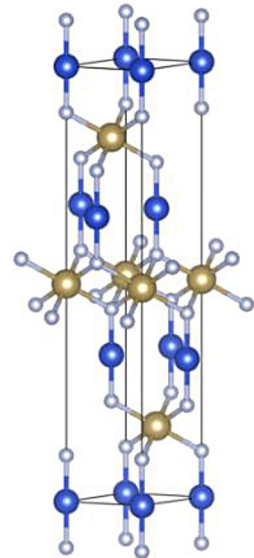
N frac	Room temperature case				200 °C case			
	Cu: Ta: N	Cu/Ta	Cu/N	Ta/N	Cu: Ta: N	Cu/Ta	Cu/N	Ta/N
0.20	1: 0.77: 2.81	1.29	0.36	0.27	1: 0.74: 2.48	1.35	0.40	0.30
0.40	1: 0.70: 2.63	1.43	0.38	0.27	1: 0.74: 2.39	1.35	0.42	0.31
0.50	1: 0.77: 2.17	1.30	0.46	0.35	1: 0.73: 2.09	1.37	0.48	0.35
0.60	1: 0.71: 2.13	1.40	0.47	0.33	1: 0.68: 2.37	1.47	0.42	0.29
0.80	1: 0.83: 1.91	1.21	0.52	0.43	1: 0.71: 2.17	1.40	0.46	0.33

Cu: Ta ratio of 1.29:1, alongside other elements (C, O, Al, and Si) at varying percentages. It's crucial to note that the SD value is independent of the ratio, reflecting the elemental composition obtained through analysis. The EDX spectra of all the CTN films revealed the presence of oxygen (in the 10 to 20% range). The presence of oxygen is a known issue in the reactive sputtering deposition of nitride films, especially when using nitrogen gas. There are two potential sources of oxygen. First, trace amounts of oxygen might have lingered within the chamber during film deposition despite attaining a better vacuum of 10^{-7} Torr before introducing the sputtering gas mixture. This residual oxygen, which is much more reactive than nitrogen, could have been incorporated into the growing CTN film. Second, the films could readily absorb oxygen molecules from the ambient atmosphere following deposition. This phenomenon is particularly likely for some metal nitride films, which often exhibit high surface reactivity [21].

Table 1 reveals several significant findings regarding the composition of the deposited thin film. The nitrogen content in the film unexpectedly decreased as the nitrogen fraction in the sputtering gas mixture increased. In contrast, copper (Cu) and tantalum (Ta) showed minimal variation across the investigated nitrogen fractions. Additionally, the Cu/Ta ratio within the film falls within the range of 1.21 to 1.43 for the room temperature case and 1.35 to 1.47 for the 200 °C case, indicating an excess of copper relative to tantalum. A deviation from the ideal 1:1 stoichiometric ratio is typical for depositing multicomponent target materials because of preferential sputtering. Preferential sputtering results from various factors, including changes in binding energies and variations in energy transfer with atomic mass. A 50/50 mixture of tantalum and copper was chosen because of the composition of CTN and because the association between yield and the causes of preferred sputtering is not well established [18, 22–24]. The results indicate that the sputtering yield of Ta is lower than that of Cu, which can be attributed to its larger atomic mass, and this difference may have been further enhanced by the higher chemical reactivity of Cu [25, 26].

For both temperature cases, using gas fractions of 0.5 N and 0.8 N resulted in film compositions that are closest to the stoichiometric composition of CTN, as shown in Table 1.

Fig. 4 Ternary copper metal nitride structures. The large dark blue (2 vertical bonds), large tan (6 bonds), and small light blue spheres represent Cu, M, and N atoms, respectively. The VESTA [28] program was used to create this illustration



3.3 XRD results

A parallel beam arrangement was used for X-ray diffraction (XRD) studies because it is known to be less susceptible to mounting problems and sample geometry [27]. A 2° angle of incidence was used, which is quite similar to the angle of total reflection of the films. Its proximity to this angle enhances the intensity of the observed XRD signal.

As mentioned in the introduction, CTN has been reported to have a delafossite structure [2, 14, 15]. This structure is also known as the rhombohedral ABC_2 structure and is a crystal structure commonly found in transition metal nitrides. It is characterized by its trigonal unit cell, which contains three layers of atoms (see Fig. 4). The first layer is composed of transition metal cations (A), the second layer is composed of nitrogen anions (C), and the third layer is composed of transition metal cations (B). In the delafossite crystal structure, the metal cations adopt a hexagonal close-packed (HCP) lattice arrangement where the anions occupy positions within an octahedral arrangement. The delafossite structure is often distorted, leading to various exciting properties.

Remarkably, the XRD patterns obtained from the films deposited at 200 °C (not shown) were indistinguishable from those deposited at room temperature. Distinct differences

were observed in the crystallinities of the CTN films based on the type of substrate on which they were deposited. The films grown on glass substrates exhibited a complete absence of crystallinity within the sensitivity range of the XRD technique. In contrast, CTN films deposited on silicon substrates are polycrystalline with a preferred orientation along the (100) direction, which matches the orientation of the silicon substrate itself. This consistent (100) orientation of both the substrate and the deposited films suggested that the substrate plays a vital role in the resulting crystalline structure and orientation of the CTN films.

The XRD diffractogram illustrated in (Fig. 5) corresponds to films deposited at room temperature on Si substrates. Given the similarity observed for the 200 °C case, this analysis is driven exclusively by the room temperature scenario. This study unveiled a complex structural composition within CTN films on Si substrates, indicating a combination of amorphous (broad humps at low angles) and crystalline regions, all of which were arranged in a delafossite-type structure. The XRD patterns further revealed distinct diffraction peaks for the CTN films prepared with varying nitrogen (N) gas ratios, with peak positions corresponding to diffraction angles of 54.46°, 54.42°, 54.10°, 53.91°, and 54.15° for N gas ratios of 0.2, 0.4, 0.5, 0.6, and 0.8, respectively. The peak for CTN in the literature was found to be at approximately 53.89° [14]. The observed peak shifts indicate subtle changes in the crystal lattice parameters, which can be linked to compositional differences. The EDX results corroborated the variations discussed in Sect. 3.2. It is worth noting that such alterations in lattice parameters are expected in sputtered films, reflecting the sensitivity of the film microstructure to deposition conditions and composition [29, 30]. There is also a relatively

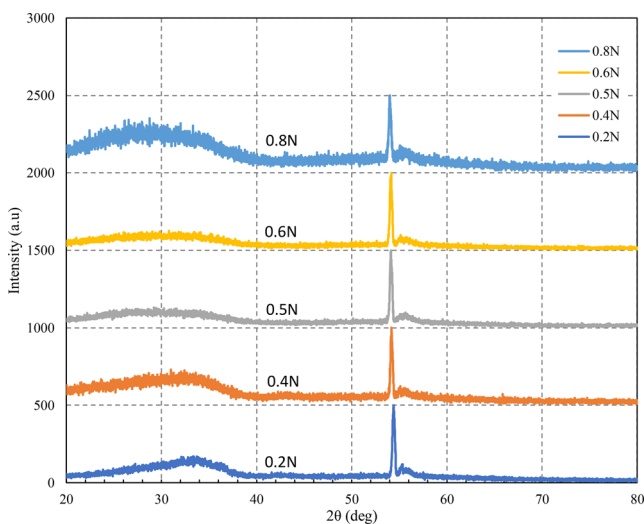


Fig. 5 XRD diffractograms of films deposited on Si substrates at different nitrogen gas fractions and room temperature

small and broad peak at approximately 55.5° from copper tantalum oxide (CuTa_2O_6) [31].

This study employed the Scherrer equation to determine the crystalline size (D) by analyzing the diffraction peaks from the obtained diffractogram [32]. The Scherrer equation is expressed as $D = \frac{k\lambda}{\beta \cos\theta}$, where D represents the crystalline size, λ is the X-ray wavelength, β is the full width at half maximum (FWHM) of the diffraction peak, θ is the diffraction angle, and k is a dimensionless shape factor. The assessment was exclusively conducted based on single identified diffraction peaks. Shape factor and X-ray wavelength values of 0.9 and 1.54059 Å (Cu) are utilized for the Scherrer equation. The calculated crystalline size using this method was determined to be approximately 30 nm. The obtained values exhibit remarkable consistency across the analyzed samples. Despite the observed variations in grain size through SEM images, these discrepancies are attributed to the accumulation of crystals, which form grains that differ at various deposition rates and are influenced explicitly by gas ratios.

The XRD patterns obtained from films deposited at different N fractions and substrate temperatures were indistinguishable; therefore, no significant crystallinity variations were revealed among all the samples deposited under various conditions. However, the subsequent Raman spectroscopy section presents further insights into the molecular structure of the film material.

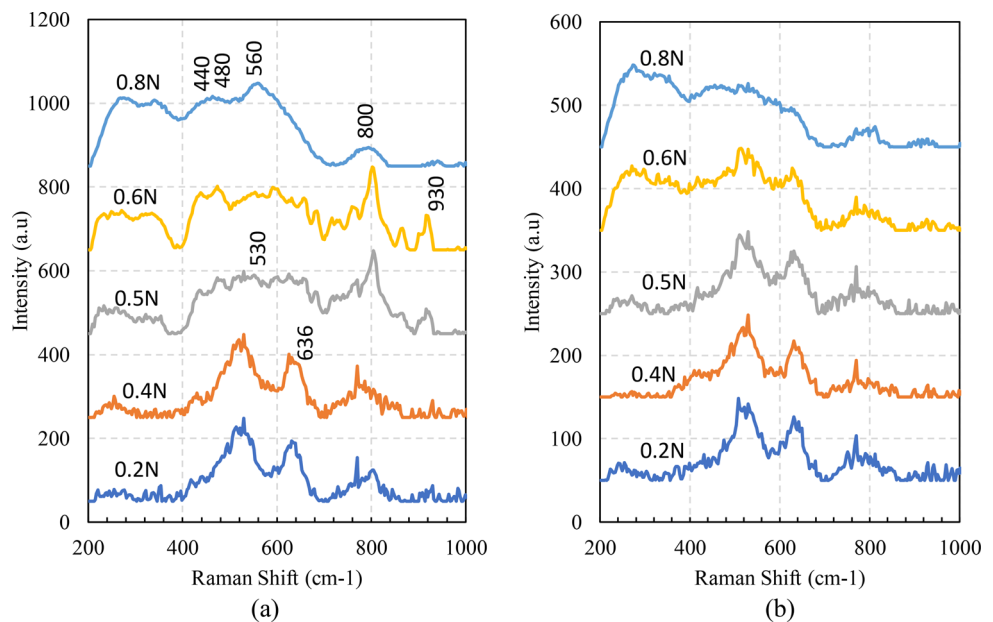
3.4 Raman analysis

Raman spectra from samples deposited on glass and Si substrates were compared with the copper and tantalum nitride spectra collected on the same tool. Raman data for the related oxides: copper oxide, cuprous oxide, and tantalum oxide [33–37], were also compared. Due to the presence of a sharp, strong peak in the spectrum attributed to the Si substrate (centered at approximately 521 cm^{-1}) compared to that of the glass substrate sample, only the spectra from the glass substrate samples are presented and analyzed here.

The Raman spectra of the deposited films revealed the absence of sharp peaks, indicative of a relatively disordered film structure. These findings complement the observations from the XRD analysis in Sect. 3.3, further corroborating the lack of significant crystallinity.

However, distinct broad peaks were observed at approximately 440, 480, and 560 cm^{-1} for CTN films deposited at nitrogen fractions of 0.2 N, 0.5 N, 0.6 N, and 0.8 N at room temperature, respectively (see Fig. 6). These peaks are not characteristic of either oxides or typical binary nitrides. Moreover, their intensity positively correlated with the nitrogen fraction employed during deposition.

Fig. 6 Raman spectra of films deposited on glass substrates at different N fractions. **(a)** Room temperature case **(b)** 200 °C case



Interestingly, films deposited with higher nitrogen fractions also displayed enhanced transparency (obtained from spectrophotometry measurements, as presented in the next Sect. 3.5) with an Urbach tail, suggesting the presence of a well-ordered structure. This observation corroborates the findings in Sect. 3.2, which indicated that higher nitrogen fractions promote improved film quality. Additionally, the spectra revealed broader peaks at approximately 530 and 636 cm^{-1} , attributable to binary nitrides. The intensity of these peaks decreased with increasing nitrogen fraction, suggesting a greater propensity for ternary phase formation at higher nitrogen contents. Additionally, other prominent peaks at approximately 270, 340, 800, and 930 cm^{-1} are found in the spectra of binary nitrides (and oxides, which are very close in the Raman shift).

On the other hand, the Raman spectra of the films deposited at a substrate temperature of 200 °C exhibit some notable differences from those deposited at room temperature (Fig. 6). While the characteristic peaks identified for CTN are present in both spectra, the absence of the distinct peak at 560 cm^{-1} observed for the 0.8 N film deposited at room temperature is noteworthy. Apart from this missing peak, the overall spectral features appear broadly similar, albeit with slightly more noise in the 200 °C film. Additionally, the intensities of several CTN peaks appear somewhat weaker than those of their counterparts in the room-temperature film.

A possible explanation for these observations lies in the increased oxidation that can occur at higher deposition temperatures. The enhanced reactivity at 200 °C could lead to a greater degree of oxide formation alongside the CTN phase. This could, in turn, mask the contributions from nitride

vibrations to the Raman spectrum, reducing the prominence of the corresponding peaks.

3.5 Spectrophotometry measurements

The band gap is essential in most potential applications of these materials. Solar cell applications, for example, could benefit from bandgap values in the 0.5 eV to approximately 2.9 eV range, depending on the specific function of the material.

The films obtained in this work have a semitransparent dark reddish color, and (Fig. 7) presents the UV–VIS–IR transmission spectra of CTN thin films deposited on glass substrates at various N fractions. Notably, the film thickness ranged from 290 to 355 nm. Below the visible range, light transmission was minimal. Marginal transmission occurred just above 300 nm, followed by a steady increase in wavelength. The 350–900 nm range exhibited interference-related maxima and minima. Films deposited with 0.5 N, 0.6 N, and 0.8 N fractions (high N fractions) displayed high visible and near-infrared optical transmission, contrasting with the significantly lower %T observed for the 0.2 N and 0.4 N samples across this range. This disparity can be attributed to the formation of semimetallic films at lower N fractions, arising from insufficient nitrogen to react with Cu, Ta, or Cu-Ta. Furthermore, the high-transmission region shifts to slightly higher wavelengths, decreasing the N flow, which can be attributed to the increased metal–N bonding. An increase in the transmittance with an increase in the N fraction for the 200 °C deposited films is also observed, but the transmittance and the band gap values obtained are lower than those obtained at room temperature.

Fig. 7 Optical transmittance spectra of films on glass substrates deposited at different N fractions. (a) Room temperature case (b) 200 °C case

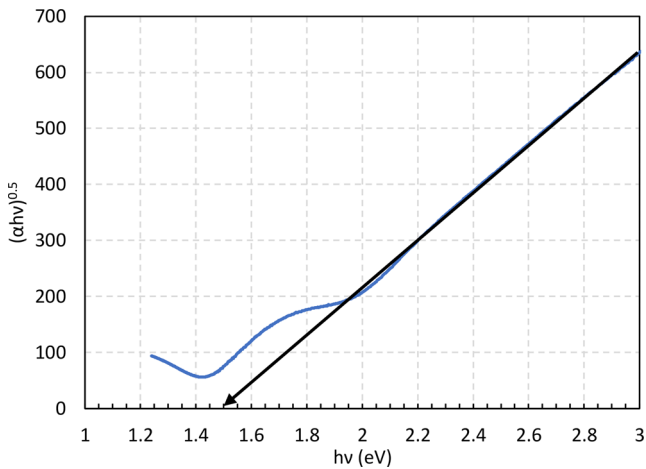
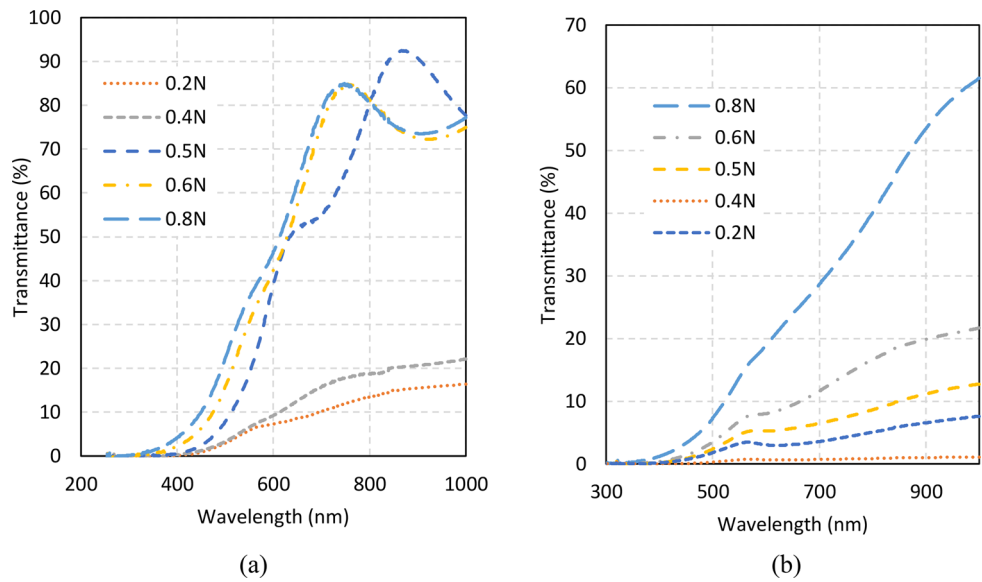


Fig. 8 A representative Tauc plot (sputtering gas nitrogen fraction 0.5)

Table 2 Bandgap values based on spectrophotometry data and Tauc plot estimates

N fraction	Band gap (eV)	
	RT case	200 °C case
0.2	1.28	0.9
0.4	1.05	1.0
0.5	1.5	1.1
0.6	1.52	1.1
0.8	1.55	1.2

A Tauc plot can be used to obtain the optical band gap of the deposited thin films [38]. The Tauc equation is $(\alpha h\nu)^m = A(h\nu - E_g)$, where α , A, h, ν , and E_g are the absorption coefficient, ordinary constant, Planck constant, photofrequency, and optical bandgap, respectively. In the case of this ternary nitride material, its indirect bandgap nature is assigned a value of $m = 1/2$. (Figure 8) shows a representative plot (for the 0.50 N fraction) depicting the relationship between

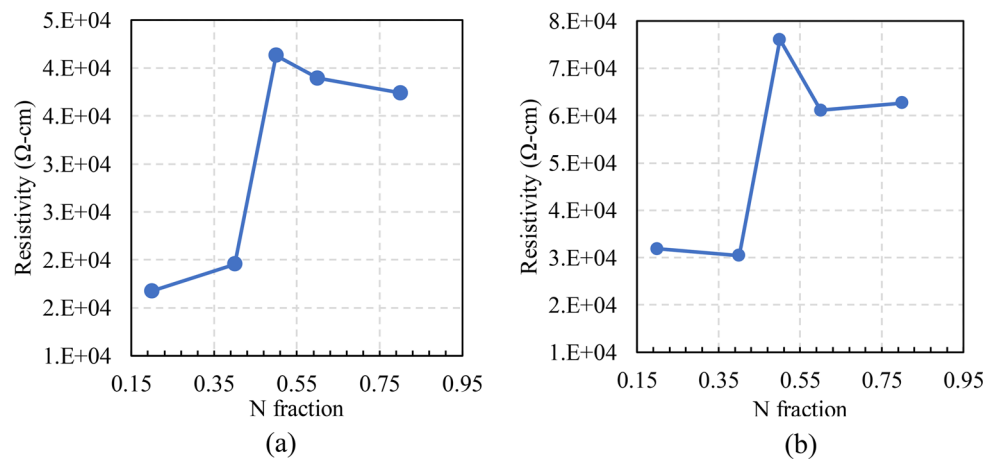
the photon energy ($h\nu$) and $(\sqrt{\alpha h\nu})$, from which the optical bandgaps were estimated through a linear fit. The diagram illustrates that the bandgap value corresponds to the photon energy where $(\sqrt{\alpha h\nu})$ equals zero. These bandgap values are tabulated in Table 2.

In this investigation, the results are compared with the limited published data on the band gap of this material. According to the literature, computational methods have estimated a range of approximately 1.3 eV to 1.4 eV [13]. First-principle computational methods often tend to underestimate the bandgap for thin-film materials. However, the sole experimentally obtained band gap reported in the literature, determined via diffuse reflectance measurements on a powder CTN sample, was 1.5 eV. The spectrophotometry-based band gap data indicate a similar trend. As determined through EDS analysis, the band gaps for closely related stoichiometric films (0.5 N, 0.6 N, and 0.8 N) are nearly 1.5 eV. Additionally, films with higher nitrogen contents exhibit lower bandgaps. In summary, the findings demonstrate that band gap values increase with increasing fraction of nitrogen in the sputtering gas mixture. Based on the spectrophotometry data, such as those presented above, the absorption coefficient for band-to-band transitions (for example, at 2.0 eV) was ordered at 10^5 cm^{-1} .

3.6 Resistivity measurements

The resistivity data for the films deposited on a glass substrate are presented next, emphasizing the dependence on the gas ratio during deposition. The resistivity measurements were conducted using the four-point probe method. The results reveal a significant variation in the resistivity with the nitrogen gas fraction in the sputtering gas mixture, as shown in (Fig. 9). Specifically, the 0.2 N fraction

Fig. 9 Resistivity as a function of the N fraction (a) Room temperature case (b) 200 °C case



exhibited the lowest recorded resistivity. This observation aligns with the broader trend, revealing a progressive increase in resistivity as the gas ratio increases to the 0.5 N fraction. Subsequently, there is a discernible decrease in resistivity as the N fraction continues to increase, though with a relatively modest magnitude. In agreement with the discussion in Sect. 3.5 (spectrophotometry), the film deposited at 0.2 N and 0.4 N appears to be more metallic (i.e., containing a more metallic phase); hence, the resistivity is low for those films and vice versa.

The measured resistivity values for the CTN films deposited at room temperature ranged from approximately 20 kΩ-cm to 45 kΩ-cm. The resistivity measurements for the film deposited at 200 °C showed values in the 30 kΩ-cm to 76 kΩ-cm range, with a trend similar to that for samples deposited at room temperature. The resistivity sharply increases above a nitrogen fraction of 0.5 N, suggesting a significant change in the electrical transport properties at higher nitrogen incorporation.

4 Conclusion

In summary, copper tantalum nitride films were deposited by RF reactive sputtering from a Cu/Ta target in a nitrogen atmosphere. The film morphology depends significantly on the deposition conditions, ranging from relatively smooth and void-free films with nanosized grains for high nitrogen content in the sputtering gas and at room temperature substrates to a structure dominated by larger submicron cauliflower-like grains with significant voids and well-defined columnar structures for low nitrogen content in the sputtering gas and elevated substrate temperature. The films were deposited using a target with a 50/50 Cu/Ta ratio found to contain less Ta than Cu. This finding implies that increasing the target Ta content is necessary to achieve a 1:1 Cu: Ta ratio in the films. Based on the XRD data, the films deposited on glass substrates are amorphous, while those deposited

on silicon substrates have a polycrystalline structure with a predominant crystalline orientation. The impact of the nitrogen fraction in the sputtering gas mixture is also significant regarding the band gap. The band gap ranges from 0.9 eV for an N fraction of 0.2 to 1.55 eV for an N fraction of 0.8. The film resistivity varies from approximately 20 kΩ-cm to 76 kΩ-cm, with a step-like increase occurring at a nitrogen fraction of 0.5 or greater. Overall, a higher nitrogen fraction results in improved semiconductor film quality—a smoother film with a larger bandgap of approximately 1.5 eV, higher resistivity of several tens of kΩ-cm, and a chemical composition that is closest to the stoichiometric CuTa_N value. This study revealed that the structure and characteristics of the films were not significantly improved by deposition at a moderately elevated substrate temperature of 200 °C. Instead, increased surface roughness characterized by larger grains and voids was observed.

Acknowledgements This work was supported by internal funding from the University of Toledo's Electrical Engineering and Computer Science (EECS) Department. The characterization work was performed at the University of Toledo's Center for Materials and Sensors Characterization (CMSC) as well as at the Wright Center for Photovoltaics Innovation and Commercialization (PVIC).

Author contributions Conceptualization: Md Maidul Islam, Daniel G. Georgiev; Methodology: Md Maidul Islam, Daniel G. Georgiev; Material preparation: Md Maidul Islam; Data collection: Md Maidul Islam, Abhishek Goud Ranga, Vamsi Borra; Data analysis: Md Maidul Islam, Abhishek Goud Ranga, Vamsi Borra, Daniel G. Georgiev; Writing: Md Maidul Islam, Daniel G. Georgiev; Review and editing: Md Maidul Islam, Daniel G. Georgiev; Visualization: Md Maidul Islam; Funding acquisition: Daniel G. Georgiev, Vamsi Borra; Supervision: Daniel G. Georgiev; All authors have read and agreed to the published version of the manuscript.

Data availability Not applicable.

Declarations

Competing interests All the authors certify that they have no affiliations with or involvement in any organization or entity with any finan-

cial or nonfinancial interest in the subject matter or materials discussed in this manuscript.

Open Access This article is licensed under a Creative Commons Attribution 4.0 International License, which permits use, sharing, adaptation, distribution and reproduction in any medium or format, as long as you give appropriate credit to the original author(s) and the source, provide a link to the Creative Commons licence, and indicate if changes were made. The images or other third party material in this article are included in the article's Creative Commons licence, unless indicated otherwise in a credit line to the material. If material is not included in the article's Creative Commons licence and your intended use is not permitted by statutory regulation or exceeds the permitted use, you will need to obtain permission directly from the copyright holder. To view a copy of this licence, visit <http://creativecommons.org/licenses/by/4.0/>.

References

1. A. Ścigała, E. Szlyk, L. Dobrzańska, D.H. Gregory, R. Szczęsny, *Coord. Chem. Rev.* **436**, 213791 (2021)
2. A. Zakutayev, *J. Mater. Chem. A* **4**, 6742 (2016)
3. W. Sun et al., *Nat. Mater.* **18**, 732 (2019)
4. H. Morkoç, *Nitride Semiconductors and Devices* (WILEY-VCH Verlag GmbH & Co., 1999), p. 1
5. M.M. Islam, D.G. Georgiev, *Appl. Phys. A* **128**, 579 (2022)
6. K. Matsuzaki, T. Katase, T. Kamiya, H. Hosono, *ACS Appl. Mater. Interfaces.* **11**, 35132 (2019)
7. A.A. Yu, R.Y. Hu, W. Liu, R. Zhang, J. Zhang, Y. Pu, L. Chu, J.P. Yang, X.A. Li, *Curr. Appl. Phys.* **18**, 1306 (2018)
8. M. Rodríguez-Tapiador, J. Asensi, M. Roldán, J. Merino, J. Bertomeu, S. Fernández, *Coatings.* **13**, 1094 (2023)
9. M.I. Rodríguez-Tapiador, J. Merino, T. Jawhari, A. Muñoz-Rosas, J. Bertomeu, S. Fernández, *Materials.* **16**, 1508 (2023)
10. C. Figueira, G.D. Rosario, D. Pugliese, M. Rodríguez-Tapiador, S. Fernández, *Materials.* **15**, 8973 (2022)
11. A. Jiang, M. Qi, J. Xiao, *J. Mater. Sci. Technol.* **34**, 1467 (2018)
12. J.-X. Zhang, Z.-Y. Zhao, *Mater. Sci. Semiconduct. Process.* **167**, 107819 (2023)
13. N. Szymanski, L. Walters, O. Hellman, D. Gall, S. Khare, *J. Mater. Chem. A* **6**, 20852 (2018)
14. U. Zachwieja, H. Jacobs, *Eur. J. Solid State Inorg. Chem.* **28**, 1055 (1991)
15. M. Yang, A. Zakutayev, J. Vidal, X. Zhang, D.S. Ginley, F.J. DiSalvo, *Energy Environ. Sci.* **6**, 2994 (2013)
16. A.H. Simon, *Handbook of thin film Deposition* (Elsevier, 2018), p. 195
17. E. Alfonso, J. Olaya, G. Cubillos, in *Crystallization-Science and technology* (2012), pp. 397
18. K. Wasa, *Handbook of Sputtering Technology*, 41 (2012)
19. M.M. Islam, D.G. Georgiev, *MRS Adv.* **7**, 523 (2022)
20. J.A. Thornton, *Journal of Vacuum Science Technology, A. Vacuum, Surfaces, and Films* **4**, 3059 (1986)
21. J.R. Xiao, M. Qi, C.Y. Gong, Z.Y. Wang, A.H. Jiang, J.F. Ma, Y. Cheng, *J. Phys. D Appl. Phys.* **51** (2018)
22. M. Seah, T. Nunnery, *J. Phys. D* **43**, 253001 (2010)
23. W. Eckstein, *Vacuum.* **82**, 930 (2008)
24. R.A. Baragiola, *Philosophical Transactions of the Royal Society of London. Ser. A: Math. Phys. Eng. Sci.* **362**, 29 (2004)
25. Tantalum vs Copper, <https://metals.compnature.com/en/tantalum-vs-copper/comparison-57-6-0> (Accessed January 5 2024)
26. H. Paul, R. Chulist, L. Lityńska-Dobrzyńska, M. Prazmowski, M. Faryna, I. Mania, Z. Szulc, M. Miszczyk, A. Kurek, *Mater. Design.* **208**, 109873 (2021)
27. A.C. Vermeulen, *Materials Science Forum* (Trans Tech Publ, 2005), p. 131
28. K. Momma, F. Izumi, *J. Appl. Crystallogr.* **41**, 653 (2008)
29. J. Xiao, M. Qi, Y. Cheng, A. Jiang, Y. Zeng, J. Ma, *RSC Adv.* **6**, 40895 (2016)
30. M. Zervos, A. Othonos, T. Pavloudis, S. Giaremis, J. Kioseoglou, K. Mavridou, M. Katsikini, F. Pinakidou, E.C. Paloura, *J. Phys. Chem. C* **125**, 3680 (2021)
31. E. Felten, *J. Inorg. Nucl. Chem.* **29**, 1168 (1967)
32. B.D.S. Cullity, S.R., in *Elements of X-Ray Diffraction* (Pearson Education Limited, England, 2014), p. 174
33. F.A. Akgul, G. Akgul, N. Yildirim, H.E. Unalan, R. Turan, *Mater. Chem. Phys.* **147**, 987 (2014)
34. L.V.A. Sayson, J.M. Lopez, E.S. Estacio, A.A. Salvador, A.S. Somintac, *Mater. Res. Express.* **6**, 125551 (2020)
35. K. Manukumar, R. Viswanatha, G. Nagaraju, *Ionics.* **26**, 1197 (2020)
36. R.R. Krishnan, K. Gopchandran, V. Mahadevan Pillai, V. Ganesan, V. Sathe, *Appl. Surf. Sci.* **255**, 7126 (2009)
37. Y. Deng, A.D. Handoko, Y. Du, S. Xi, B.S. Yeo, *ACS Catal.* **6**, 2473 (2016)
38. J. Tauc, R. Grigorovici, A. Vancu, *Phys. Status Solidi (b).* **15**, 627 (1966)

Publisher's Note Springer Nature remains neutral with regard to jurisdictional claims in published maps and institutional affiliations.